

Within-session dynamics of theta–gamma coupling and high-frequency oscillations during spatial alternation in rat hippocampal area CA1

Hiroshi Nishida · Muneyoshi Takahashi ·
Johan Lauwereyns

Received: 17 October 2013 / Revised: 24 March 2014 / Accepted: 10 April 2014 / Published online: 19 April 2014
© Springer Science+Business Media Dordrecht 2014

Abstract Theta–gamma coupling in the hippocampus is thought to be involved in cognitive processes. A large body of research establishes that the hippocampus plays a crucial role in the organization and maintenance of episodic memory, and that sharp-wave ripples (SWR) contribute to memory consolidation processes. Here, we investigated how the local field potentials in the hippocampal CA1 area adapted along with rats' behavioral changes within a session during a spatial alternation task that included a 1-s fixation and a 1.5-s delay. We observed that, as the session progressed, the duration from fixation onset to nose-poking in the choice hole reduced as well as the number of premature responses during the delay. Parallel with the behavioral transitions, the power of high gamma during the delay period increased whereas that of low gamma decreased later in the session. Furthermore, the strength of theta–gamma modulation later in the session showed significant increase as compared to earlier in the session. Examining SWR during the reward period, we found that the number of SWR events decreased as well as the power

in a wide frequency range during SWR events. In addition, the correlation between SWR and gamma oscillations just before SWR events was higher in the earlier trials than in the later trials. Our findings support the notion that the inputs from CA3 and entorhinal cortex play a critical role in memory consolidation as well as in cognitive processes. We suggest that SWR and the inputs from the two areas serve to stabilize the task behavior and neural activities.

Keywords Hippocampus · Spatial alternation · Rat · Theta rhythm · Gamma oscillations · Sharp-wave ripples

Introduction

Gamma oscillations have been observed in several regions and across species with an apparent role in cognitive processes (Herrmann et al. 2004; Jensen et al. 2007; Fries et al. 2007; Colgin and Moser 2010). Many studies have reported that gamma oscillations are associated with low-frequency band activity (i.e., cross-frequency coupling; CFC) in various areas (Rojas-Libano and Kay 2008; Tort et al. 2008; Igarashi et al. 2013; Lopez-Azcarate et al. 2013; Zheng and Zhang 2013; van Wingerden et al. 2014), suggesting that CFC may be a common computational mechanism in the brain (Canolty and Knight 2010; Buzsaki and Wang 2012; Lisman and Jensen 2013). Although CFC has commanded considerable attention from many researchers, it is poorly understood how gamma-oscillations, low-frequency band activity, and their CFC changes as a behavioral task proceeds. In the present study, we focused on transitions in the animals' behavior and neural activity in a relatively short term.

We recorded neural activity in the hippocampus, which plays a critical role in memory and learning (Squire 1992; Eichenbaum et al. 1994). In the rat hippocampus, there is a

H. Nishida · J. Lauwereyns (✉)
Graduate School of Systems Life Sciences, Kyushu University,
744 Motoooka, Nishi-ku, Fukuoka 819-0395, Japan
e-mail: jan@sls.kyushu-u.ac.jp

H. Nishida
Japan Society for the Promotion of Science, Tokyo 102-0083,
Japan

M. Takahashi · J. Lauwereyns
Brain Science Institute, Tamagawa University, Tokyo 194-8610,
Japan

J. Lauwereyns
Faculty of Arts and Science, Kyushu University,
Fukuoka 819-0395, Japan

remarkable low-frequency activity, the well-known “theta rhythm.” It has been reported that the theta rhythm modulates gamma oscillations (Bragin et al. 1995a; Tort et al. 2008; Colgin et al. 2009; Belluscio et al. 2012) and their CFC alters depending on the running speed (Chen et al. 2011; Ahmed and Mehta 2012) and the behavioral performance (Tort et al. 2009; Shirvalkar et al. 2010). Here we particularly focused on the CFC during a delay period, which several studies have suggested to require the involvement of hippocampus for successful task performance (Ainge et al. 2007; Pastalkova et al. 2008; Takahashi et al. 2009a, b; MacDonald et al. 2011).

On the other hand, hippocampal high-frequency oscillation, accompanied with large-amplitude irregular activity (sharp-wave ripples, SWR), is thought to be involved in memory consolidation processes (Buzsaki 1986, 1989). SWR occurs during a reward period after successful behavior and during post-learning sleep with hippocampal cell reactivation (Wilson and McNaughton 1994; Foster and Wilson 2006). Selective elimination of SWR results in memory deficits on hippocampus-dependent spatial tasks (Girardeau et al. 2009; Jadhav et al. 2012). Furthermore, a recent study has reported that gamma oscillations co-occurred with SWR and might support the dynamic formation of coordinated CA3 and CA1 cell assemblies (Carr et al. 2012). It has been suggested that these activities reflect neural mechanisms toward the updating of memory. However, it remains unclear how the current information is reconstructed on the basis of memory in relation to behavioral stabilization in a short period.

To address these issues, we analyzed the local field potentials (LFP) from the hippocampal CA1 as rats performed a memory-guided spatial alternation task that included a 1-s fixation period and a 1.5-s delay period (Takahashi et al. 2009a, b). Although the rats were well-trained for the spatial choice on the alternation task, we expected that the rats' behavior and hippocampal activities would change during the delay period in a behavioral session, in accordance with recent findings that the hippocampus plays a critical role during precisely such delayed periods (Ainge et al. 2007; Pastalkova et al. 2008; MacDonald et al. 2011). In addition, if SWR and gamma oscillations contribute to memory consolidation or behavioral stabilization, these activities should show some transient changes within sessions, relating to the transitions of behavior and hippocampal activities.

Methods

Experimental setup

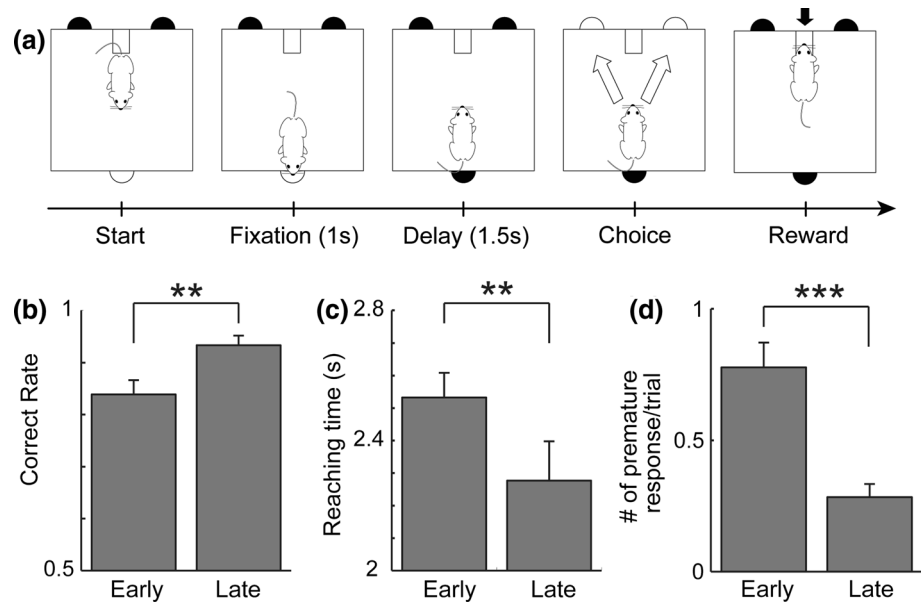
The experimental chamber was constructed using Plexiglas with black wallpaper to reduce the scattered reflection of

light. A head-stage was used for position tracking (40 × 40 × 40 cm). The front wall of the chamber included nose-poke holes on the right and on the left, and the reward port with a food dispenser (PD-25D; O'hara & Co., Ltd., Tokyo, Japan) delivered 25-mg food pellets (O'hara & Co., Ltd., Tokyo, Japan). The rear wall included a nose-poke hole in the center. These nose-poke holes were 2 cm in diameter and 2 cm in depth. LEDs attached to the holes were used as visual cues. A 0.5 s buzzer sound was presented at the time of reinforcer delivery. A CCD camera was mounted on the ceiling of the sound-attenuating box for monitoring and position tracking.

Four male Wistar/ST rats (weighing 280–420 g; 16–24 weeks old at the beginning of training; Japan SLC Inc., Hamamatsu, Japan) were used as subjects. The rats were trained on a delayed spatial memory-guided alternation task that included a 1-s fixation period and a 1.5-s delay period (Takahashi et al. 2009a, b), as illustrated in Fig. 1a. At the beginning of a trial, the rat had to keep nose poking for 1 s (Fixation). After that, there was a 1.5-s delay period. Trials continued even if the rat responded during the delay. However, if the rat entered a choice port before the choice cues turned on, the rat had to wait for another second from the response. The LEDs in the choice ports turned on immediately after the delay, and the rat had to choose the right or left hole (alternating the choice on a trial-by-trial basis). All events were controlled by customized software developed with Microsoft Visual C++ 6.0 on a Windows-based personal computer. A daily session lasted 60 min. The training was considered complete when the rat was able to perform at an accuracy rate of >80 % and with a total of >100 correct trials during three consecutive sessions.

After training sessions, the rats were implanted with 14-tetrode hyperdrives (Neuro-hyperdrive; David Kopf Instruments, Tujunga, CA) that allow independent vertical movement of each drive (Wilson and McNaughton 1993). The Cheetah 160 Data Acquisition System (Neuralynx, Bozeman, MT) was used to record neural activity and behavioral events. The hyper-drive was connected to a headstage with 54 unity-gain preamplifiers. The neural activity at the most prominent channel of each tetrode was band-pass filtered (1–475 Hz), differentially amplified (2,000×), digitized at 2 kHz, and then stored to the hard disk as LFP data. For position tracking, the position of the ten LEDs on the headstage was detected by a CCD camera placed directly above the experimental chamber. The median point of these ten LEDs was calculated and recorded to disk at 60 Hz. The spatial sampling resolution was such that a pixel was approximately equivalent to 1 mm. The center of the electrode bundle was positioned for the dorsal CA1 pyramidal cell layer (3.6 mm posterior to bregma and 2.2 mm right-lateral to midline) in

Fig. 1 **a** Delayed spatial alternation task. **b–d** Comparison of behavior between earlier and later trials; **b** Correct performance rate for the spatial choice. **c** Duration from fixation onset to choice response. **d** Number of premature response per trial. In all figures, *error bars* indicate SEM, and ** indicates $p < 0.005$ and *** indicates $p < 0.001$ on Mann–Whitney U test



accordance with the brain atlas (Paxinos and Watson 2005). The rats were given 5 days to recover from the surgery before resuming the behavioral sessions. All procedures were in accordance with the U. S. National Institutes of Health guidelines for animal care and approved by the Tamagawa University Animal Care and Use Committee.

After all recording sessions had been completed, the rats were deeply anesthetized with an overdose of sodium pentobarbital (120 mg/kg, ip) and a 30-A anodal current was passed for 5 s through one channel for each of the 12 tetrodes. The rats were then perfused transcardially, initially with normal saline, subsequently with 10 % formalin. Coronal sections (50 μ m) were cut with a cryostat (CM3050S; Leica Microsystems, Nussloch, Germany) and stained with cresyl violet. The locations of electrode tips and tracks in the brain were identified on the basis of a stereotaxic atlas (Paxinos and Watson 2005).

Data analysis

To investigate how the rats' behavior changed within a session, we investigated the correct choice rate, the duration from fixation onset to choice response, and the number of premature responses during the delay period. As for the running speed of the rats, we filtered the position tracking data with a 20-ms window, using Gaussian smoothing, before the calculation of the running speed.

For the analysis of LFP, we used neural data during correct trials, that is, with the appropriate alternation choice. The frequency bands of low gamma, high gamma, and SWR were defined as 30–45, 60–90, and 150–250 Hz, respectively. For the first step of processing of LFP, we

eliminated the direct current offset and slow fluctuations using MATLAB (MathWorks, Natick, MA), and the *locdetrend* function in Chronux 2.00 toolbox (Bokil et al. 2010).

We calculated the power spectrum for 1 s around the choice and the specific peak frequency of the theta rhythm. To examine gamma band activities around the choice period, we calculated the power spectrogram, using a 300-ms window with 30-ms steps, before and after the rats made a nose-poking response to the correct choice hole. The power spectrogram was normalized by the mean and the standard deviation of the power time series in each behavioral session.

To examine the phase–amplitude coupling between theta and gamma oscillations, we computed normalized amplitude average of gamma based on theta phase in each 20° bin for 1 s around choice (positive polarity upward). We then calculated a synchronization index (Cohen 2008), using a 500-ms window with 50-ms steps, to quantify strength of transient phase–amplitude coupling between the theta rhythm and gamma oscillations around the choice period. For the first step of processing for both analyses, LFP was filtered to obtain the theta rhythm, which showed a peak in the power spectrum for 1 s around choice (8–10 Hz), and gamma oscillations. As for gamma oscillations, LFP was filtered with a narrow band-pass, with 2 Hz steps from 30 to 100 Hz. The envelope of the narrow-band signal was calculated after applying the Hilbert transformation, and filtered by the theta band to extract theta-modulated components of gamma amplitude. The instantaneous phase of the theta rhythm φ_θ and the envelope φ_γ were calculated after applying the Hilbert transformation. The synchronization index $SI_{\theta\gamma}$ was obtained by

$$SI_{\theta\gamma} = \frac{1}{N} \left| \sum_{n=1}^N \exp(i(\varphi_{\theta}(n) - \varphi_{\gamma}(n))) \right|$$

where N is the number of time-points during each time window and i is a complex number. We converted $SI_{\theta\gamma}$ using the Fisher z-transformation ($0.5 \times \log([1 + SI_{\theta\gamma}]/[1 - SI_{\theta\gamma}])$), with values ranging from 0 to 1 in order to approximate a normal distribution. We then conducted t tests to compare the values in gamma bands before and after choice in the earlier and later trials.

We analyzed the LFP for the 10-s ITI period after the rat chose the correct hole, and while it remained in the half side of the box that included the reward point. SWR events were detected when the 10-ms Gaussian filtered envelope of the filtered LFP (150–250 Hz) exceeded the mean + 3SD for at least 15 ms. For the purpose of analyzing SWR associated with eating, we eliminated the data points for which the running speed was over 4 cm/s. We calculated SWR-triggered spectrograms using MATLAB (MathWorks, Natick, MA) and Chronux toolbox 2.00 (Bokil et al. 2010). The window had a width of 100-ms and moved with 10-ms steps. The padding factor was 2. The power spectrogram was normalized at each frequency band by the mean and standard deviation in each behavioral session. To confirm the relationship between low gamma and SWR in accordance with a previously-published protocol (Carr et al. 2012), we calculated the Pearson's correlation coefficient. For more detailed analysis, we computed the amplitude-comodulation index before and after detecting SWR events between 30 and 300 Hz oscillations. The comodulation index was calculated by the following formula (Masimore et al. 2004):

$$\rho_{ij} = \frac{\sum_k (S_k(f_i) - \langle S(f_i) \rangle)(S_k(f_j) - \langle S(f_j) \rangle)}{\sigma_i \sigma_j}$$

where $S_k(f_i)$ represents the spectral density at frequency f_i in time-window k , $\langle S(f_i) \rangle$ the average spectral density magnitude at frequency f_i over all time-windows, σ_i the standard deviation of the spectral density at frequency f_i , and k ranges over all the time-windows.

Results

Analysis of behavioral changes within a session

We collected data from 18 behavioral sessions (112.4 trials per session with a standard deviation, SD, of 34.9). For the purpose of investigating within-session dynamics of the rats' behavior, we used 180 trials (18 session \times the first 10 trials) for the early period and 180 trials (18 session \times the last 10 trials) for the late period, and compared behavioral

measures between the earlier and the later trials. As shown in Fig. 1b–d, we found that the rats' behavior changed significantly in a session even though the rats were well trained for spatial alternation. First, we confirmed that the correct choice rate in the later trials was higher than in earlier trials (Fig. 1b; $p < 0.005$ by Mann–Whitney U test; 0.84 ± 0.03 vs 0.93 ± 0.01 ; Mean \pm SEM). In addition, the duration from fixation onset to choice response (Fig. 1c; $p < 0.005$ by Mann–Whitney U test; 2.53 ± 0.19 vs 2.28 ± 0.12 ; Mean \pm SEM) and the number of premature responses during the delay period reduced in later trials (Fig. 1d; $p < 0.001$ by Mann–Whitney U test; 0.78 ± 0.09 vs 0.28 ± 0.05 ; Mean \pm SEM). Thus, the rats seemed to perform the behavioral task more accurately and quickly after adjusting during the session.

Analysis of theta rhythm and gamma oscillations around choice

We next examined the neural activity obtained from 31 electrodes located in hippocampal CA1 area and used 310 trials (31 electrodes \times the first 10 trials) for the early period and 310 trials (31 electrodes \times the last 10 trials) for the late period. At first, we computed the power spectrum of theta band activity for 1 s around choice. As shown in Fig. 2a, the peak of the power for the theta rhythm was around 9 Hz in both phases of a session, but with a statistically significant difference (Fig. 2b left; $p < 0.01$ by unpaired two tailed t test; 8.68 ± 0.05 vs 8.87 ± 0.04 ; Mean \pm SEM). The power of the theta rhythm (6–12 Hz) around choice did not show a significant difference between the early and the late trials (Fig. 2b right; $p > 0.4$ by unpaired two tailed t test; 6.13 ± 0.19 vs 6.00 ± 0.16 ; Mean \pm SEM). Upon examining the gamma oscillations around the choice period (Fig. 2c–e), we found that, as compared to the later session, high gamma increased significantly before the choice (Fig. 2d left side; $p < 0.01$ by unpaired two tailed t test; 0.46 ± 0.03 vs 0.61 ± 0.04 ; Mean \pm SEM) and after the choice (Fig. 2d right side; $p < 0.01$ by unpaired two tailed t test; 0.58 ± 0.03 vs 0.73 ± 0.04 ; Mean \pm SEM), whereas low gamma showed a significant decrease before the choice (Fig. 2e left side; $p < 0.05$ by unpaired two tailed t test; -0.09 ± 0.03 vs -0.19 ± 0.03 ; Mean \pm SEM) but not after the choice (Fig. 2e right side; $p > 0.1$ by unpaired two tailed t test; 0.13 ± 0.04 vs 0.05 ± 0.04 ; Mean \pm SEM).

We next examined the phase–amplitude coupling between theta rhythm and gamma oscillations around choice. Figure 3a shows that high gamma was phase-locked to the peak of the theta rhythm whereas low gamma was phase-locked to the trough of the theta rhythm. Furthermore, the modulation depth at all frequency bands was higher in later trials than in earlier trials. We then

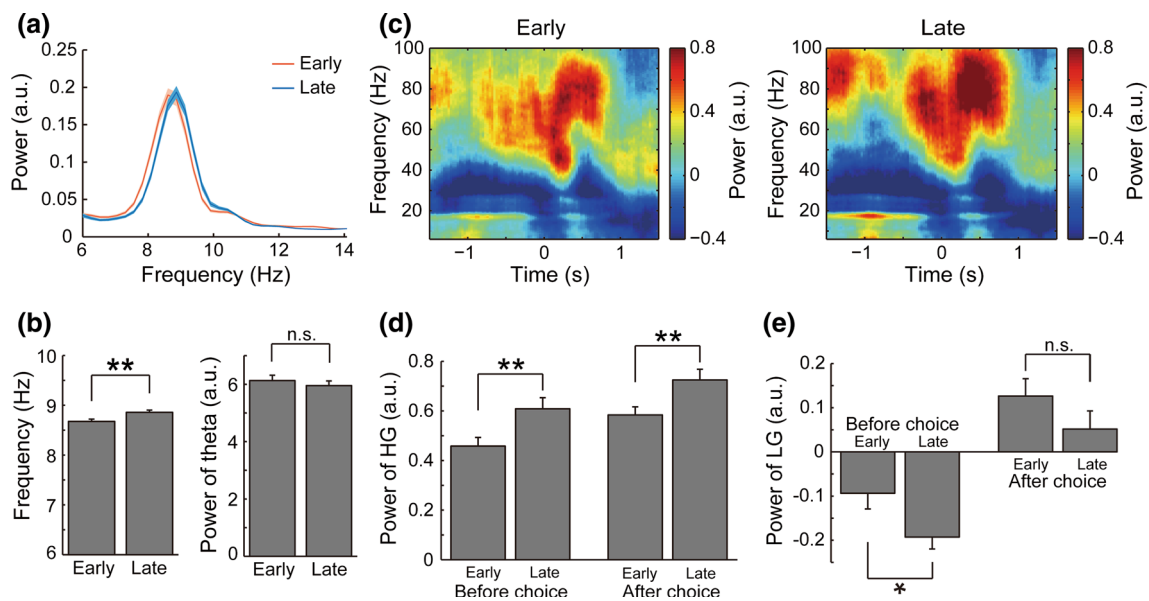


Fig. 2 Comparisons of theta and gamma oscillations between earlier and later trials around choice. **a** Power spectrum in the theta band for 1 s around choice. *Solid lines* indicate the mean and *colored areas* indicate SEM. **b** Peak frequency and mean power of the theta rhythm (6–12 Hz) for 1 s around choice. **c** Power spectrogram for 3 s around choice (± 1.5 s). **d, e** Mean power of high gamma (60–90 Hz) and low

gamma (30–45 Hz) for 0.5 s before choice and 0.5 s after choice, respectively. In all figures, *error bars* indicate SEM, and * indicates $p < 0.05$ and ** indicates $p < 0.01$ by unpaired two tailed *t* test. HG and LG in the figures mean high and low gamma, respectively. (Color figure online)

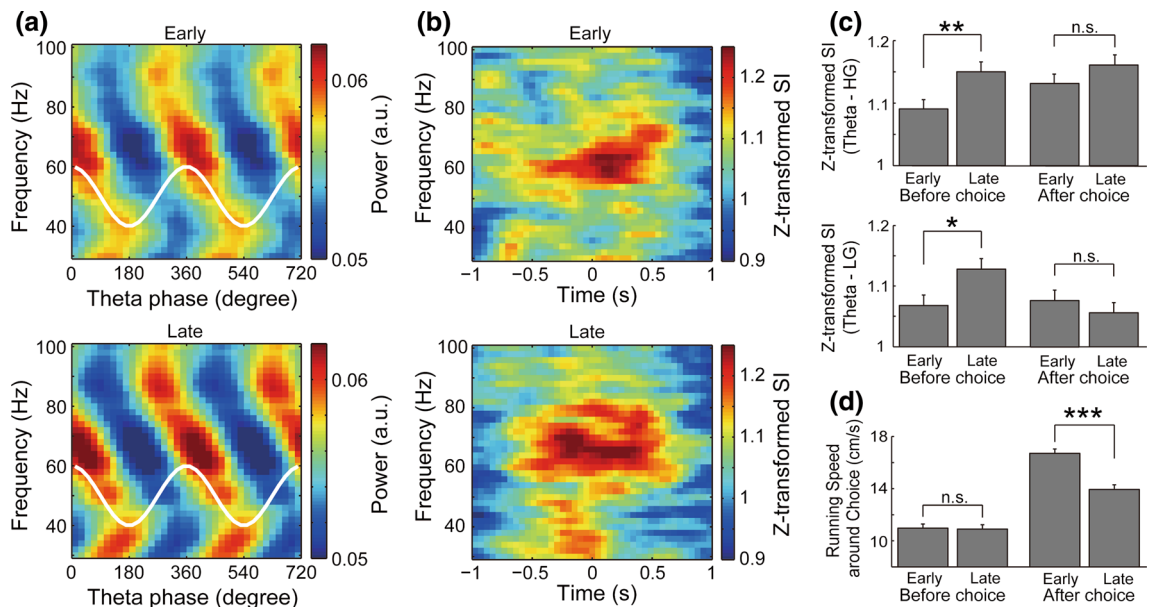


Fig. 3 The dynamics of the theta phase modulation of hippocampal gamma oscillations. **a** Normalized power average of gamma oscillations based on the phase of theta rhythm (8–10 Hz) for 1 s around choice (± 0.5 s). The *white line* shows the theta phase (with positive polarity upward). **b** Normalized synchronization index (NSI) for 2 s around choice. 0 s in the *horizontal axis* indicates the choice timing.

c Mean ZSI of high gamma (HG; 60–90 Hz)—theta rhythm (TH; 8–10 Hz) and low gamma (LG; 30–45 Hz)—TH for 0.5 s before choice and 0.5 s after choice, respectively. * indicates $p < 0.05$ and ** indicates $p < 0.01$ by unpaired two tailed *t* test. **d** Running speed for 0.5 s before and after choice. *** indicates $p < 0.001$ by Mann–Whitney U test. In all figures, *error bars* indicate SEM

computed a synchronization index, converted by a Fisher z-transformation (ZSI), between theta band and gamma band activities around the choice in the earlier and the later

trials (Fig. 3b). We compared the ZSI between the earlier trials and the later trials for each time and frequency bin (Fig. 3c). For the theta rhythm, we used an 8–10 Hz band

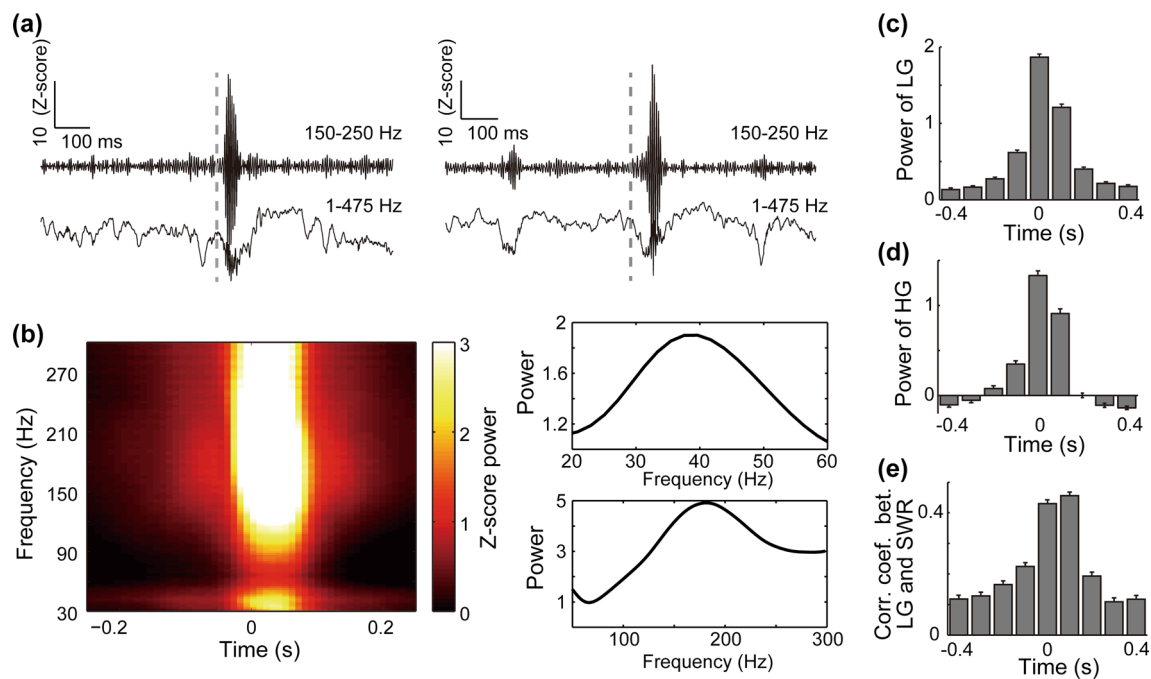


Fig. 4 **a** Examples of SWR; the *upper signal* was filtered between 150 and 250 Hz, the *lower signal* was non-filtered (1–475 Hz). A *vertical dashed line* indicates the detection of SWR. **b–e** Results following a previous protocol (Carr et al. 2012). **b** SWR-triggered power spectrogram. 0 s on the *horizontal axis* represents the moment when an SWR was detected. The *right figures* show the mean power

of low gamma in the SWR range (*upper*) and the high gamma range (*lower*) over 100 ms after SWR detection. **c**, **d** Mean power of low gamma in **c** and high gamma in **d** in each 100-ms bin. **e** Correlation coefficient between SWR and low gamma. HG and LG in the figures mean high and low gamma, respectively. Again, 0 s on the *horizontal axis* represents the moment when an SWR was detected

filtered signal, that is, around the peak in theta band power as according to Fig. 2a. Figure 3c shows that, compared to the earlier trials, ZSI significantly increased in high and low gamma bands before the choice in the later trials (high gamma, $p < 0.01$ by unpaired two tailed t test, 1.09 ± 0.01 vs 1.15 ± 0.02 ; low gamma, $p < 0.05$ by unpaired two tailed t test, 1.07 ± 0.02 vs 1.12 ± 0.02 ; mean \pm SEM) but not after the choice (high gamma, $p > 0.1$ by unpaired two tailed t test, 1.13 ± 0.01 vs 1.16 ± 0.02 ; low gamma, $p > 0.4$ by unpaired two tailed t test, 1.08 ± 0.02 vs 1.05 ± 0.02 ; Mean \pm SEM).

Many studies have shown that theta rhythm, gamma oscillations and the cross-frequency coupling change depending on running speed (Vanderwolf 1969; Chen et al. 2011; Ahmed and Mehta 2012). Then, we investigated the rats' running speed around the choice period. As shown in Fig. 3d, there was no statistical difference between the earlier and the later trials before the choice period ($p > 0.8$; 10.97 ± 0.32 vs 10.91 ± 0.33 ; Mean \pm SEM) while the running speed after the choice showed a significant decrease later in the session ($p < 0.001$ by Mann–Whitney U test; 16.71 ± 0.34 vs 13.94 ± 0.36 ; Mean \pm SEM). Thus, the changes of the power of gamma oscillations and the coupling strength before choice could not be explained by the running speed.

Analysis of sharp-wave ripples and gamma oscillations during the reward period

To investigate high and low gamma oscillations during SWR events, we extracted SWR events and then calculated the SWR-triggered power spectrogram following the protocol (Carr et al. 2012) as shown in Fig. 4a,b. Consistent with their study, we observed that the power of the gamma oscillations increased toward SWR events (Fig. 4b–d). Furthermore, we also found that the low gamma oscillations correlated positively with SWR, again similar to the previous study (Fig. 4e).

Subsequently, we investigated whether the neural oscillations during SWR adapted to the behavioral transitions. First, we compared the number of SWR events per trial in the earlier and the later trials, dividing the data into the first 10 trials and the last 10 trials in a session. As shown in Fig. 5a, SWR events occurred more often in the earlier trials than in the later trials ($p < 0.001$ by Mann–Whitney U test; 0.24 ± 0.01 vs 0.16 ± 0.01 ; Mean \pm SEM). We then examined the power difference around SWR events between the first 10 and the last 10 times of SWR in each session (Fig. 5b). After computing the mean power spectrogram in the earlier and later SWRs, we calculated the power difference by subtracting the mean

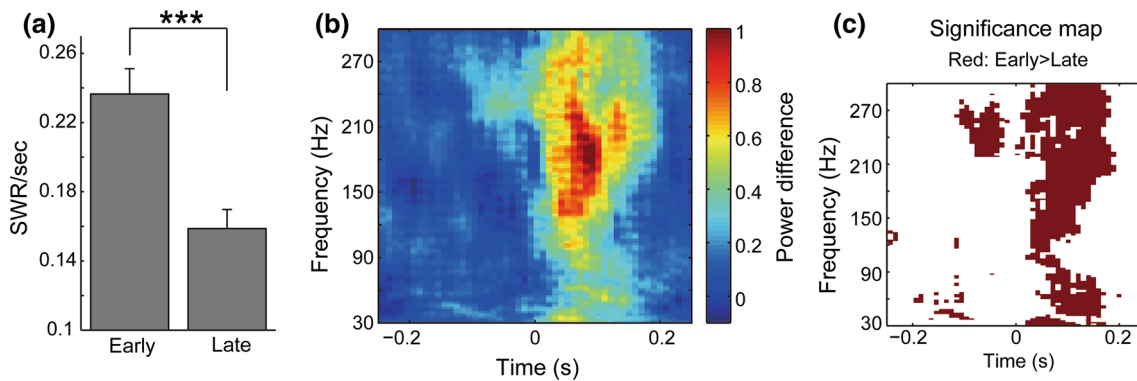


Fig. 5 **a** Number of SWR events per trial in earlier trials and later trials. *** indicates $p < 0.001$ by Mann–Whitney U test. **b** The power difference between earlier and later trials (subtracting the power in later trials from that in earlier trials). 0 s on the horizontal axis indicates the detection of an SWR. Red indicates that the power is

higher in earlier trials than in later trials. **c** Significance map with statistically significant results ($p < 0.05$) between earlier and later trials by Mann–Whitney U test. Red indicates that the power is significantly higher in earlier trials than in later trials. (Color figure online)

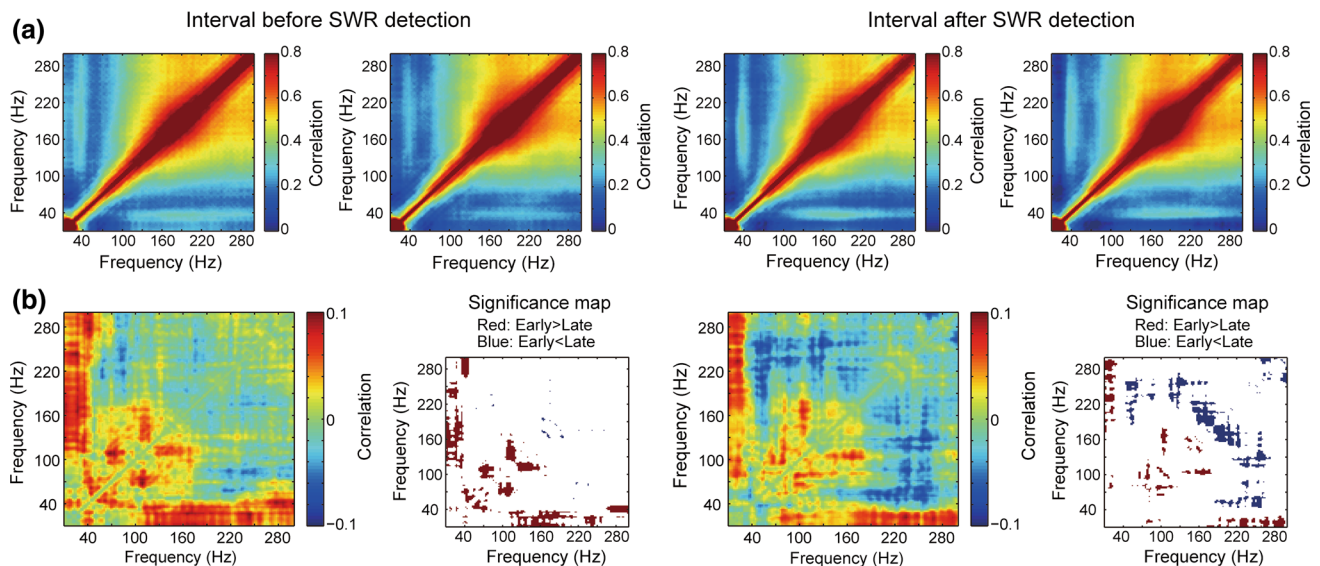


Fig. 6 Comparison of amplitude comodulation between earlier and later SWRs. The data are shown for 0.1 s before SWR detection (panels in the left half of the figure) and for 0.1 s after SWR detection (panels in the right half of the figure). **a** Amplitude comodulogram plot. **b** Comodulation difference between the earlier and the later SWRs; subtraction of comodulation index in the later SWRs from that

in the earlier SWRs. The significance map shows whether the difference between the comodulation index in the earlier versus the later SWRs is statistically significant. Red indicates that the comodulation index in the earlier SWRs is significantly higher than in the later SWRs; blue indicates the opposite. (Color figure online)

power in the later SWRs from that in the earlier SWRs. Figure 5c shows that a large fraction of the mean power in the earlier SWRs after detecting SWR events was significantly higher than that in the later SWRs, especially in the SWR frequency band.

To investigate how the relationship between gamma oscillations and SWR changed within a session, we drew the amplitude-comodulogram for 100 ms before and after detection of SWR (Fig. 6a,b). Consistent with previous results, the positive correlation between low gamma and

SWR increased around SWR events (Figs. 4e, 6a). Differences in the correlation just before SWR events above the gamma band were observed in three frequency pairs; low gamma oscillation and wide-frequency bands, high gamma oscillation and high frequency oscillation (HFO; 90–120 Hz), HFO and SWR (Fig. 6b). On the other hand, just after SWR events, the correlation between low gamma oscillation and SWR in the earlier trials was lower than in the later trials, while the other correlations remained high in the earlier trials.

Discussion

In the present study, we found that rats' behavior during the delay periods changed within a daily session although the rats were well-trained for the spatial choice. Associated with the behavioral changes, we found several types of neural dynamics within a session: theta–gamma modulation before the choice, and, during the reward period, SWR and gamma oscillations, including in the high frequency oscillation band.

There are two major projections from entorhinal cortex (EC) to hippocampus. One is a part of the hippocampal trisynaptic circuit (EC – Dentate Gyrus – CA3 – CA1) (Andersen et al. 1969), and the other is the direct projection from EC to CA1 through the temporoammonic pathway (Steward and Scoville 1976). It is known that the external inputs to the hippocampus are associated with high gamma oscillation (60–90 Hz), whereas the internal hippocampal signals from CA3 to CA1 are associated with low gamma oscillation (30–45 Hz) (Bragin et al. 1995a; Colgin et al. 2009).

In line with the anatomical scheme, the increase of high gamma around choice in the later session may reflect the stronger input from EC, which is projected from many cortical areas (Canto et al. 2008) and may receive the majority of sensory information, whereas the decrease of low gamma may be affected by the lower input from CA3, which may be involved in pattern completion (Nakazawa et al. 2002). On the other hand, the strength of theta–gamma modulation increased in the majority of frequency bands in the later trials. By examining the running speed around the choice, we were able to confirm that at least the changes before the choice were not due to running speed. The increase in the coupling may be caused by synaptic plasticity in the CA1–CA3 and CA1–EC network (Xu et al. 2013a, b), suggesting optimization of the communication between neural groups in these regions (Fries 2005; Singer 2009). Considering the putative functional roles in the different hippocampal areas and the behavioral changes during the delay period as a result of adjusting to the behavioral task (i.e. the reduction of premature responses and reaction times), we hypothesize that the rats are able to minimize their deliberative decision-making about which direction they should choose (hence the decrease of low gamma, and less energy required from CA3), and instead focus already on the next step in processing their choice, that is, paying attention to the relevant external stimuli (i.e. the timing of the illumination of the choice hole; hence the increase of high gamma, and more reliance on input from EC).

SWR could contribute to the changes of neural activities required for cognitive processing. SWR is thought to result from a synchronized burst in the hippocampal CA3 region

(Buzsaki et al. 1983). It also has been shown that the temporoammonic (TA) pathway is crucial for the consolidating process (Remondes and Schuman 2004). We observed decreasing trends of power in a wide range of frequency bands during SWR. Interpreting this result, the input strength from EC and CA3, and the number of activated neurons in CA1 during SWR might decrease, optimizing the neural grouping with respect to the behavioral demands. Consequently, the number of SWRs that exceed the threshold would reduce as well. Furthermore, our results showed that the correlation between high gamma (which reflects input from EC) and HFO (which might be lower frequency SWR) changed in the earlier trials as compared to the later trials. Although our results suggest that the input via the TA pathway is involved in memory consolidation processes and the occurrence of SWR, sharp wave-associated bursts increased after lesion of EC (Bragin et al. 1995b). Thus, the interaction and the input timing from these areas might be critical for the generation of SWR and consolidation.

In sum, in the present study we showed how neural activities in rat hippocampal area CA1 around the choice point and during SWR adapted along with behavioral changes. Our findings support the notion that the inputs from CA3 and entorhinal cortex play a critical role in memory consolidation as well as in cognitive processes. Particularly, we suggest that SWR and the inputs from the two areas serve to stabilize the task behavior and neural activities.

Acknowledgments This work was supported by Human Frontier Science Program award RGP0039/2010, KAKENHI (24120710; Neural creativity for communication), Tamagawa GCOE Program, Narishige Neuroscience Research Foundation, and Grant-in-Aid for JSPS Fellows.

References

- Ahmed OJ, Mehta MR (2012) Running speed alters the frequency of hippocampal gamma oscillations. *J Neurosci Off J Soc Neurosci* 32(21):7373–7383. doi:10.1523/JNEUROSCI.5110-11.2012
- Ainge JA, van der Meer MA, Langston RF, Wood ER (2007) Exploring the role of context-dependent hippocampal activity in spatial alternation behavior. *Hippocampus* 17(10):988–1002. doi:10.1002/hipo.20301
- Andersen P, Bliss TV, Lomo T, Olsen LI, Skrede KK (1969) Lamellar organization of hippocampal excitatory pathways. *Acta Physiol Scand* 76(1):4A–5A
- Belluscio MA, Mizuseki K, Schmidt R, Kempter R, Buzsaki G (2012) Cross-frequency phase–phase coupling between theta and gamma oscillations in the hippocampus. *J Neurosci Off J Soc Neurosci* 32(2):423–435. doi:10.1523/JNEUROSCI.4122-11.2012
- Bokil H, Andrews P, Kulkarni JE, Mehta S, Mitra PP (2010) Chronux: a platform for analyzing neural signals. *J Neurosci Methods* 192(1):146–151. doi:10.1016/j.jneumeth.2010.06.020

- Bragin A, Jando G, Nadasdy Z, Hetke J, Wise K, Buzsaki G (1995a) Gamma (40–100 Hz) oscillation in the hippocampus of the behaving rat. *J Neurosci Off J Soc Neurosci* 15(1 Pt 1):47–60
- Bragin A, Jando G, Nadasdy Z, van Landeghem M, Buzsaki G (1995b) Dentate EEG spikes and associated interneuronal population bursts in the hippocampal hilar region of the rat. *J Neurophysiol* 73(4):1691–1705
- Buzsaki G (1986) Hippocampal sharp waves: their origin and significance. *Brain Res* 398(2):242–252
- Buzsaki G (1989) Two-stage model of memory trace formation: a role for “noisy” brain states. *Neuroscience* 31(3):551–570
- Buzsaki G, Wang XJ (2012) Mechanisms of gamma oscillations. *Annu Rev Neurosci* 35:203–225. doi:10.1146/annurev-neuro-062111-150444
- Buzsaki G, Leung LW, Vanderwolf CH (1983) Cellular bases of hippocampal EEG in the behaving rat. *Brain Res* 287(2):139–171
- Canolty RT, Knight RT (2010) The functional role of cross-frequency coupling. *Trend Cogn Sci* 14(11):506–515. doi:10.1016/j.tics.2010.09.001
- Canto CB, Wouterlood FG, Witter MP (2008) What does the anatomical organization of the entorhinal cortex tell us? *Neural Plast.* doi:10.1155/2008/381243
- Carr MF, Karlsson MP, Frank LM (2012) Transient slow gamma synchrony underlies hippocampal memory replay. *Neuron* 75(4):700–713. doi:10.1016/j.neuron.2012.06.014
- Chen Z, Resnik E, McFarland JM, Sakmann B, Mehta MR (2011) Speed controls the amplitude and timing of the hippocampal gamma rhythm. *PLoS ONE* 6(6):e21408. doi:10.1371/journal.pone.0021408
- Cohen MX (2008) Assessing transient cross-frequency coupling in EEG data. *J Neurosci Methods* 168(2):494–499. doi:10.1016/j.jneumeth.2007.10.012
- Colgin LL, Moser EI (2010) Gamma oscillations in the hippocampus. *Physiology* 25(5):319–329. doi:10.1152/physiol.00021.2010
- Colgin LL, Denninger T, Fyhn M, Hafting T, Bonnevie T, Jensen O, Moser MB, Moser EI (2009) Frequency of gamma oscillations routes flow of information in the hippocampus. *Nature* 462(7271):353–357. doi:10.1038/nature08573
- Eichenbaum H, Otto T, Cohen NJ (1994) Two functional components of the hippocampal memory system. *Behav Brain Sci* 17(03):449–472. doi:10.1017/S0140525X00035391
- Foster DJ, Wilson MA (2006) Reverse replay of behavioural sequences in hippocampal place cells during the awake state. *Nature* 440(7084):680–683. doi:10.1038/nature04587
- Fries P (2005) A mechanism for cognitive dynamics: neuronal communication through neuronal coherence. *Trend Cogn Sci* 9(10):474–480. doi:10.1016/j.tics.2005.08.011
- Fries P, Nikolic D, Singer W (2007) The gamma cycle. *Trends Neurosci* 30(7):309–316. doi:10.1016/j.tins.2007.05.005
- Girardeau G, Benchenane K, Wiener SI, Buzsaki G, Zugaro MB (2009) Selective suppression of hippocampal ripples impairs spatial memory. *Nat Neurosci* 12(10):1222–1223. doi:10.1038/nn.2384
- Herrmann CS, Munk MH, Engel AK (2004) Cognitive functions of gamma-band activity: memory match and utilization. *Trend Cogn Sci* 8(8):347–355. doi:10.1016/j.tics.2004.06.006
- Igarashi J, Isomura Y, Arai K, Harukuni R, Fukai T (2013) A theta-gamma oscillation code for neuronal coordination during motor behavior. *J Neurosci Off J Soc Neurosci* 33(47):18515–18530. doi:10.1523/JNEUROSCI.2126-13.2013
- Jadhav SP, Kemere C, German PW, Frank LM (2012) Awake hippocampal sharp-wave ripples support spatial memory. *Science* 336(6087):1454–1458. doi:10.1126/science.1217230
- Jensen O, Kaiser J, Lachaux JP (2007) Human gamma-frequency oscillations associated with attention and memory. *Trends Neurosci* 30(7):317–324. doi:10.1016/j.tins.2007.05.001
- Lisman JE, Jensen O (2013) The theta-gamma neural code. *Neuron* 77(6):1002–1016. doi:10.1016/j.neuron.2013.03.007
- Lopez-Azcarate J, Nicolas MJ, Alegre M, Valencia M, Artieda J (2013) Delta-mediated cross-frequency coupling organizes oscillatory activity across the rat cortico-basal ganglia network. *Front Neural Circ* 7:155. doi:10.3389/fncir.2013.00155
- MacDonald CJ, Lepage KQ, Eden UT, Eichenbaum H (2011) Hippocampal “time cells” bridge the gap in memory for discontinuous events. *Neuron* 71(4):737–749. doi:10.1016/j.neuron.2011.07.012
- Masimore B, Kakaliotis J, Redish AD (2004) Measuring fundamental frequencies in local field potentials. *J Neurosci Methods* 138(1–2):97–105. doi:10.1016/j.jneumeth.2004.03.014
- Nakazawa K, Quirk MC, Chitwood RA, Watanabe M, Yeckel MF, Sun LD, Kato A, Carr CA, Johnston D, Wilson MA, Tonegawa S (2002) Requirement for hippocampal CA3 NMDA receptors in associative memory recall. *Science* 297(5579):211–218. doi:10.1126/science.1071795
- Pastalkova E, Itskov V, Amarasingham A, Buzsaki G (2008) Internally generated cell assembly sequences in the rat hippocampus. *Science* 321(5894):1322–1327. doi:10.1126/science.1159775
- Paxinos G, Watson C (2005) *The rat brain in stereotaxic coordinates*, 5th edn. Elsevier Academic Press, Amsterdam
- Remondes M, Schuman EM (2004) Role for a cortical input to hippocampal area CA1 in the consolidation of a long-term memory. *Nature* 431(7009):699–703. doi:10.1038/nature02965
- Rojas-Libano D, Kay LM (2008) Olfactory system gamma oscillations: the physiological dissection of a cognitive neural system. *Cogn Neurodyn* 2(3):179–194. doi:10.1007/s11571-008-9053-1
- Shirvalkar PR, Rapp PR, Shapiro ML (2010) Bidirectional changes to hippocampal theta-gamma comodulation predict memory for recent spatial episodes. *Proc Natl Acad Sci USA* 107(15):7054–7059. doi:10.1073/pnas.0911184107
- Singer W (2009) Distributed processing and temporal codes in neuronal networks. *Cogn Neurodyn* 3(3):189–196. doi:10.1007/s11571-009-9087-z
- Squire LR (1992) Memory and the hippocampus: a synthesis from findings with rats, monkeys, and humans. *Psychol Rev* 99(2):195–231
- Steward O, Scoville SA (1976) Cells of origin of entorhinal cortical afferents to the hippocampus and fascia dentata of the rat. *J Comp Neurol* 169(3):347–370. doi:10.1002/cne.901690306
- Takahashi M, Lauwereyns J, Sakurai Y, Tsukada M (2009a) Behavioral state-dependent episodic representations in rat CA1 neuronal activity during spatial alternation. *Cogn Neurodyn* 3(2):165–175. doi:10.1007/s11571-009-9081-5
- Takahashi M, Lauwereyns J, Sakurai Y, Tsukada M (2009b) A code for spatial alternation during fixation in rat hippocampal CA1 neurons. *J Neurophysiol* 102(1):556–567. doi:10.1152/jn.91159.2008
- Tort AB, Kramer MA, Thorn C, Gibson DJ, Kubota Y, Graybiel AM, Kopell NJ (2008) Dynamic cross-frequency couplings of local field potential oscillations in rat striatum and hippocampus during performance of a T-maze task. *Proc Natl Acad Sci USA* 105(51):20517–20522. doi:10.1073/pnas.0810524105
- Tort AB, Komorowski RW, Manns JR, Kopell NJ, Eichenbaum H (2009) Theta-gamma coupling increases during the learning of item-context associations. *Proc Natl Acad Sci USA* 106(49):20942–20947. doi:10.1073/pnas.0911331106
- van Wingerden M, van der Meij R, Kalenschers T, Maris E, Pennartz CM (2014) Phase-amplitude coupling in rat orbitofrontal cortex discriminates between correct and incorrect decisions during associative learning. *J Neurosci Off J Soc Neurosci* 34(2):493–505. doi:10.1523/JNEUROSCI.2098-13.2014

- Vanderwolf CH (1969) Hippocampal electrical activity and voluntary movement in the rat. *Electroencephalogr Clin Neurophysiol* 26(4):407–418
- Wilson MA, McNaughton BL (1993) Dynamics of the hippocampal ensemble code for space. *Science* 261(5124):1055–1058
- Wilson MA, McNaughton BL (1994) Reactivation of hippocampal ensemble memories during sleep. *Science* 265(5172):676–679
- Xu X, An L, Mi X, Zhang T (2013a) Impairment of cognitive function and synaptic plasticity associated with alteration of information flow in theta and gamma oscillations in melamine-treated rats. *PLoS ONE* 8(10):e77796. doi:[10.1371/journal.pone.0077796](https://doi.org/10.1371/journal.pone.0077796)
- Xu X, Zheng C, Zhang T (2013b) Reduction in LFP cross-frequency coupling between theta and gamma rhythms associated with impaired STP and LTP in a rat model of brain ischemia. *Front Comput Neurosci* 7:27. doi:[10.3389/fncom.2013.00027](https://doi.org/10.3389/fncom.2013.00027)
- Zheng C, Zhang T (2013) Alteration of phase–phase coupling between theta and gamma rhythms in a depression-model of rats. *Cogn Neurodyn* 7(2):167–172. doi:[10.1007/s11571-012-9225-x](https://doi.org/10.1007/s11571-012-9225-x)